ARTICLES SCIENCE CHINA Materials

mater.scichina.com link.springer.com

Published online 16 May 2017 | doi: 10.1007/s40843-017-9041-0
Sci China Mater 2017, 60(7): 654–663

Bimetallic organic frameworks derived CuNi/carbon nanocomposites as efficient electrocatalysts for oxygen reduction reaction

Sisi Wu, Yinggang Zhu, Yifeng Huo, Yaocong Luo, Lihua Zhang, Yi Wan, Bo Nan, Lujie Cao, Zhenyu Wang, Minchan Li, Mingyang Yang, Hua Cheng and Zhouguang Lu*

ABSTRACT Catalysts of oxygen reduction reaction (ORR) play key roles in renewable energy technologies such as metal-air batteries and fuel cells. Despite tremendous efforts, highly active catalysts with low cost remain elusive. This work used metal-organic frameworks to synthesize non-precious bimetallic carbon nanocomposites as efficient ORR catalysts. Although carbon-based Cu and Ni are good candidates, the hybrid nanocomposites take advantage of both metals to improve catalytic activity. The resulting molar ratio of Cu/Ni in the nanocomposites can be finely controlled by tuning the recipe of the precursors. Nanocomposites with a series of molar ratios were produced, and they exhibited much better ORR catalytic performance than their monometallic counterparts in terms of limited current density, onset potential and half-wave potential. In addition, their extraordinary stability in alkaline is superior to that of commercially-available Pt-based materials, which adds to the appeal of the bimetallic carbon nanocomposites as ORR catalysts. Their improved performance can be attributed to the synergetic effects of Cu and Ni, and the enhancement of the carbon matrix.

Keywords: electrocatalysts, oxygen reduction reaction, metal organic frameworks, non-precious metal, nanocomposites

INTRODUCTION

Increasing energy demands have prompted the intense investigation of sustainable, alternative energy conversion and storage systems with high efficiency and low cost, such as metal-air batteries and fuel cells [1,2]. A lack of highly active but low-cost electrocatalysts of oxygen reduction reaction (ORR) is one of the major bottlenecks for the progress in such energy systems [2–4]. Presently, Pt-based materials are the best-known ORR catalysts because of their high efficiency, but are limited to a great extent by their prohibitive cost and low stability [4–6]. In this regard, a broad range of abundant and less expensive materials, including non-precious metals and metal-free materials, have been actively explored as catalysts for oxygen reduction [7–9]. More recently, heteroatom-doped carbon-supported materials have been considered the most promising substitutes for platinum [10–12]. The heteroatoms, especially nitrogen, have the inclination to form heteroatom-metal active sites and increase catalytic efficiency during oxygen reduction [10,13]. In addition, the graphitization of the porous carbon matrix enhances electrical conductivity and therefore the catalytic performance [14,15]. However, in spite of tremendous efforts, ideal materials with excellent electrochemical activity and durability are yet to be developed. The major difficulty lies in the intrinsic catalytic activity, active sites and the poor mass transport of the potential materials [16]. Current approaches to improving such materials include the tuning of active sites and the construction of nanostructures [17–19]. Therefore, despite some progress, the development of alternatives to Pt-based materials as ORR catalysts remains a huge challenge.

Porous carbons have captured great attention in a wide range of applications including electrode materials, gas storage/separation, water purification and catalyst support [20–23]. The large surface area and low cost, together with good chemical stability and electrical conductivity, have made various porous carbon extensively-studied materials in the field of electrochemistry. Among all kinds of porous carbon materials, metal-organic frameworks (MOFs) are a class of hybrid functional materials, which have high

Department of Materials Science and Engineering, Southern University of Science and Technology, Shenzhen 518055, China
* Corresponding author (email: luzg@sustc.edu.cn)

surface area, porosity and tuning potential [24,25]. Constructed from metal centers and organic linkers of great diversity, their nanoscale cavities and open structures make MOFs the ideal precursors for conversion into functional nanostructures [26,27]. The weak thermal stability of MOFs makes it possible to preserve their porous structure, uniform element distribution, and high porosity when transformed into porous carbon *via* pyrolysis [15,26,28]. Thus, MOF-derived catalysts have been the actively studied materials with comparable or better ORR catalytic performance than Pt-based catalysts [14,15,29]. Among them, transition metals in porous carbon matrix have been regarded promising to replace Pt-based materials. In such materials, the porous carbon matrix greatly enhances the electron transfer efficiency and prevents metal aggregations [30]. In recent years, carbon-based bimetallic ORR catalysts appear and have swiftly become widely studied. Although the hybrid of precious metal and non-precious metal presents excellent performance [31,32], alloys of different non-precious metals, for instance, CuFe, FeCo, CuCo and ZnCo [14,33–35], also have potential because of the abundance and low cost. However, no studies have developed efficient nanocomposites that incorporate Cu and Ni as ORR catalysts. To the best of our knowledge, although Cu is not an active ORR catalyst compared to the most efficient non-noble materials, copper based enzymes are famous for their oxygen reduction reactivity [36–39]. On the other hand, the extensively-studied PtM (M is transition metal such as Ni, Fe, Co) [40–42] demonstrates enhanced kinetics of the ORR than the commercial Pt/C.

Bearing this in mind, we successfully synthesized a series of bimetallic MOFs based on previous work [43], with different ratios of Cu/Ni (denoted as CuNi-DABCO-n, where n refers to the copper concentration in the metal components). These CuNi-DABCOs served as precursors to bimetallic carbon nanocomposites (CuNi/C-n, where n again refers to Cu content), and a simple pyrolysis helped all the MOF-derived CuNi/C-n inherit porous carbon from the precursor to provide a large surface area and high graphitization degree. Remarkably, the optimized sample exhibits much better ORR catalytic performance than the individual counterparts in terms of both diffusion-limited current density and onset potential. In addition, the better long-term stability in alkaline solution than Pt/C also makes it a promising catalyst for oxygen reduction.

EXPERIMENTAL SECTION

Preparation of CuNi-DABCO-n

The synthesis of Cu-DABCO and Ni-DABCO were based on the previous study [43]. The fabrication of bimetallic precursors CuNi-DABCO-n involved certain modification. Typically, the raw materials including $Cu(NO_3)_2{\cdot}3H_2O$, $Ni(NO_3)_2{\cdot}6H_2O$, 1,4-benzene dicarboxylate (BDC) and 1,4-diazabicyclo[2.2.2]octane (DABCO) were dissolved in 60 mL of dimethyl formamide (DMF). Keeping the total amount of the nitrate salt (3 mmol) constant, the two nitrate salts were added at the desired molar ratio of Cu/Ni, which varied from 0.3 to 9. The mixture was then stirred vigorously for 20 min, followed by sonication for 20 min. Thereafter, the mixture was transferred into a Teflon-lined autoclave and heated to 120°C for 48 h. The product was separated by centrifugation and washed thoroughly with DMF for three times to completely remove the residual DMF and unreacted reagents. Finally, the product was dried overnight at 60°C prior to further use.

Preparation of CuNi/C-n

The precursors obtained above were annealed under a mixed gas flow containing 5% hydrogen and 95% argon, at 700°C for 5 h with a heating rate of 2°C min^{-1}. The products were then allowed to cool to room temperature.

Investigation of electrocatalytic performance

All electrochemical measurements were performed in a typical three-electrode system in 0.1 mol L^{-1} KOH solution. A glassy carbon (GC) electrode of 5 mm diameter (0.1963 cm^{-2} in surface area) served as the substrate of the working electrode. A platinum wire and a saturated Hg/HgO electrode were used as the counter and reference electrodes, respectively. To prepare the working electrode, 10 mg of the catalyst was dispersed in 1 mL of a mixture (containing 90% ethanol and 10% 5 wt.% Nafion solution). The mixture was then sonicated for 30 min to form a well-dispersed ink and 10 μL of it was dropped onto the GC surface with a pipette, with a 0.5 mg cm^{-2} loading concentration for all catalysts, and dried in the ambient environment. Prior to evaluation of every sample, a continuous flow was bubbled through the electrolyte for 30 min to saturate it with Ar/O_2. The cyclic voltammetry (CV) and rotating disk electrode (RDE) measurements were performed in Ar and O_2-saturated 0.1 mol L^{-1} KOH at a scan rate of 10 mV s^{-1} at room temperature, while linear sweep voltammetry (LSV) required the rotation speed to range from 400 to 2500 rpm. For comparison, commercial Pt-based material (Pt/C, 20 wt.% platinum) was prepared and tested in the same way. All potentials in this work were referenced to the reversible hydrogen electrode (RHE). In 0.1 mol L^{-1} KOH, E (RHE) = E (Hg/HgO) + 0.862 V.

For ORR catalytic efficiency, the Koutecky-Levich (K-L) equation was used to calculate the electron transfer number, n:

$$\frac{1}{i} = \frac{1}{i_k} + \frac{1}{i_d}, \quad (1)$$

$$i_k = nFA\kappa C_{O_2}, \quad (2)$$

$$i_d = 0.620nFAC_{O_2}D_{O_2}^{2/3}\nu^{-1/6}\omega^{1/2} = K\omega^{1/2}, \quad (3)$$

where i is the current density obtained from the RDE measurement; i_k and i_d are the kinetic and diffusion-limiting currents, respectively; n represents the molar number of transferred electrons with respect to reactive species; F (96,500 C mol^{-1}) is the Faraday constant; A (0.1963 cm^{-2}) is the effective surface area of the working electrode; κ is the electron-transferred rate constant; C_{O_2} (1.2×10^{-6} mol cm^{-3}) and D_{O_2} (1.9×10^{-5} cm^2 s^{-1}) represent the bulk concentration and diffusion coefficient of oxygen in 0.1 mol L^{-1} KOH solution at room temperature, respectively; ν is the kinetic viscosity of the electrolyte (0.01 cm^2 s^{-1}); ω is the angular velocity of the working electrode ($\omega = 2\pi N$, where N is the linear rotation speed); and K refers to the reciprocal of the slope of the K-L curves.

RESULTS AND DISCUSSION

The bimetallic catalysts were synthesized *via* a facial two-step procedure (Scheme 1). All the precursors were synthesized by a solvothermal method based on the reported study [43] with modification. As the molar ratio of Cu/Ni increased, the obtained CuNi/C experienced a gradual color evolution from cyan to light green (Fig. S1), while the color of all products from one batch remained consistent. This gradual color evolution firmly indicates the metal ratio variation in the three dimensional (3D) structure, and also the ratio control obtained by tuning the metal source during precursor synthesis. This can also be verified by the X-ray diffraction (XRD) patterns (Fig. S2) of all precursors as the similar peaks remained with different content of copper. For some reason, the crystallinity of the MOFs are not good and the peak at ca. 6° for the pure Cu-DABCO is lost. A possible explanation could be the impurity induced when stirring and harvesting the product. The precise Cu/Ni ratios were further characterized by inductively coupled plasma mass spectrometry (ICP-MS). As the representative, the result of CuNi-DABCO-80 was measured to be 84, which is quite close to the feed number. The scanning electron microscopy (SEM) images demonstrate the morphology and surface characteristics of all precursors with various metal ratios (Fig. S3). The monometallic precursor Ni-

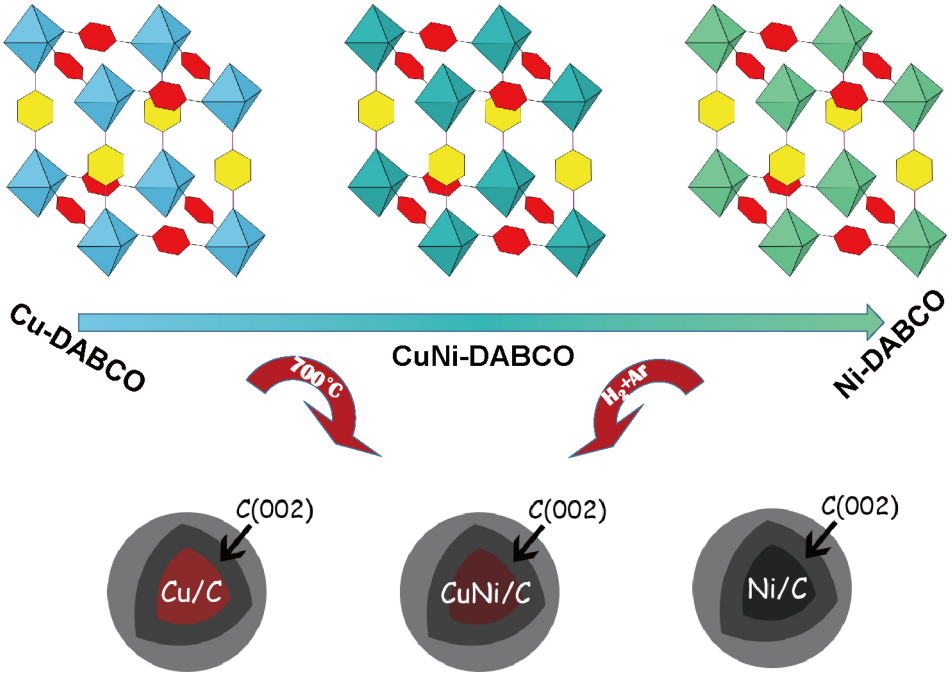

Scheme 1 Schematic illustration of the synthesis procedure of the CuNi/C-n.

DABCO has a sheet-like morphology (Fig. S3a), while the Cu-DABCO exhibits a rod or needle-like shape, and most of them are stacked together, forming a layered morphology (Fig. S3g). In addition, the prepared Ni-DABCO and Cu-DABCO samples have much smaller particle sizes of around 200 nm. With increasing copper ratios, the nanoparticles experience a gradual evolution from uniform sheets to stacked, cube-like particles, followed by a transformation to rod or needle shapes. Particle sizes also change with Cu ratio, growing from 200 nm (Fig. 1a and Fig. S3a) to ~700 nm (Fig. S3e), then back to 200 nm again (Fig. S3g).

The CuNi/C-n catalysts were obtained by pyrolysis of the prepared CuNi-DABCO-n precursors at 700°C in a mixed gas environment (5% H_2, 95% Ar). The temperature was selected to both completely decompose the MOF framework [43] and avoid further agglomeration or particle size growth [44]. The SEM images of CuNi/C-80 (Fig. 1b), as a representative of the bimetallic carbon catalysts, show well-dispersed nanoparticles with an average particle size of 150 nm. This nanoscale particle size, which is much smaller than that of the precursor, can be attributed to the decomposition of the MOF framework and vaporization of gaseous species during pyrolysis. This small particle size to some extent increases the surface area and improves electrochemical performance. The transmission electron microscopy (TEM) images of CuNi/C-80 reveal a well-dispersed bimetallic nanoparticle in the porous carbon, without much aggregation (Fig. 1c, d). The high-resolution TEM (HRTEM) (Fig. 1e) suggests that the two metal elements were well alloyed, since the interplane spacing of the (111) crystal lattice (~0.207 nm) is between the values of the typical fcc Cu (0.209 nm, PDF#04-0836) and Ni (0.204 nm, PDF#04-0850). The selected area electron diffraction

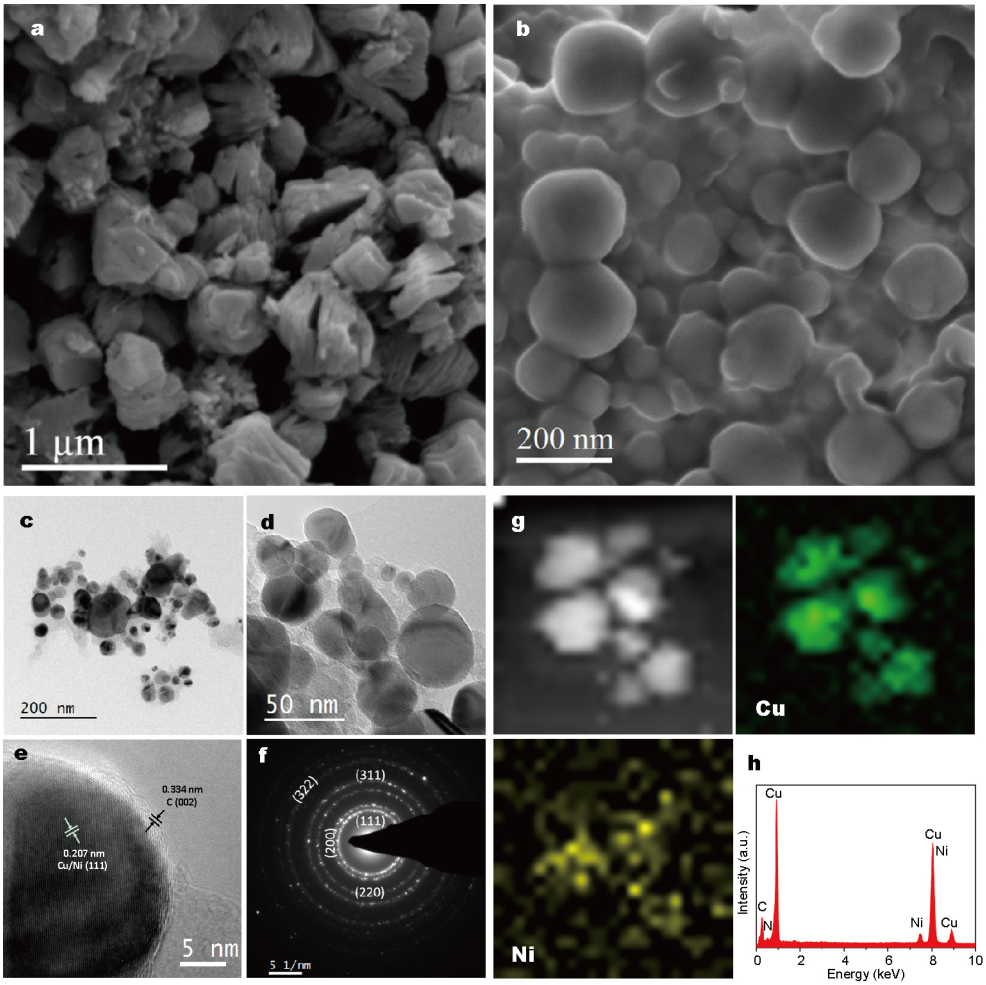

Figure 1 SEM images of (a) CuNi-DABCO-80 and (b) CuNi/C-80. (c) Low magnification and (d) high magnification TEM images of CuNi/C-80. (e) HRTEM image of CuNi/C-80 showing the graphitized carbon covering crystalline bimetallic nanoparticles. Corresponding (f) SAED pattern and (g) elemental mapping of Cu and Ni. (h) EDX spectrum of CuNi/C-80.

(SAED) result (Fig. 1f) demonstrates more specific bimetallic lattice information—it contains other fcc planes besides (111)—while all the interplane spacings are within the values of pure Cu and Ni. A shell of (002) graphitized carbon around the bimetallic particle can be easily identified with an interlayer spacing of 0.334 nm (Fig. 1e) [45]. The graphitized carbon encapsulating the bimetallic nanoparticles helps provide extra stability and durability during the further investigation of electrocatalysis [46]. This carbon graphitization must come from the presence of transition metal Ni and Cu during the pyrolysis at high temperature [47]. Furthermore, the elemental mapping of CuNi/C-80 as a representative (Fig. 1g) proves the uniform and highly dispersed metal distribution in the carbon matrix after pyrolysis, which indicates a proper heating process that avoids particle aggregation and allows synergetic effects in oxygen reduction catalysis. The TEM-energy dispersive X-ray (EDX) spectrum (Fig. 1h) suggests a slight presence of nitrogen and carbon in addition to the alloys, which may contribute to the excellent catalytic performance.

The XRD patterns (Fig. 2a) reveal the composition of the MOF-derived CuNi/C-n. The patterns are aligned with respect to the increasing copper ratio. Each pattern exhibits two strong peaks which can be indexed to (111) and (200) diffractions of either fcc Cu or fcc Ni, or in between. Comparatively, the peaks' intensities are much lower for the bimetallic samples than Ni/C and Cu/C. This is because of the distortion of the precursor structure by the introduction of the second metal element. It is important to note that, with rising copper ratios, the peaks shift negatively and approach the Cu/C peaks. The shift in the XRD peaks indicates a consistent, gradual increase in copper composition before and after pyrolysis. The shift is due to the lattice expansion and shrinkage with the changing ratio of the introduced second metal element. Together with the similar results in the interplane spacing measured in HRTEM and SAED, the peak shifts verify the formation of alloys, instead of monometallic nanoparticles. The graphitization degree of the carbon matrix is proved by the Raman spectra (Fig. 2b). The ratio of I_G/I_D increases with increasing copper ratio, with CuNi/C-80 attaining the maximum. The high graphitization degree comes from the presence of transition metals during pyrolysis [47] and facilitates the excellent catalytic performance of the bimetallic nanoparticles.

Surface area and pore distribution were investigated by N_2 sorption/desorption measurements at 77 K. The CuNi-DABCO-80 sample exhibits a reversible type-IV adsorption isotherm (Fig. 3a), suggesting the concurrent existence of micropores and macropores. The initial steep increase before 0.02 P/P_0 suggests a quick volumetric uptake in the pores. The following platform at relatively low pressure is indicative of micropore filling. The slight hysteresis between adsorption and desorption branches suggests the existence of mesopores [48], although few of them were characterized in the pore size distribution, and micropores make up the majority of pores (Fig. 3b). Fig. 3b indicates that the pores in CuNi-DABCO-80 are generally within the micropore range, with diameters smaller than 3 nm. The bimetallic MOF reaches a surface area of 289.4 $m^2 g^{-1}$, which is one order smaller than that reported for Cu-DABCO and Ni-DABCO in the reference work [43]. A possible explanation could also be the introduction of the second metal element and, therefore, the distortion of the framework structure. After pyrolysis, the resulting bimetallic catalysts shrank in surface area (52.7 $m^2 g^{-1}$) due to pore ruptures and, therefore, particle agglomeration. Certain changes also occurred to the pore size distribution

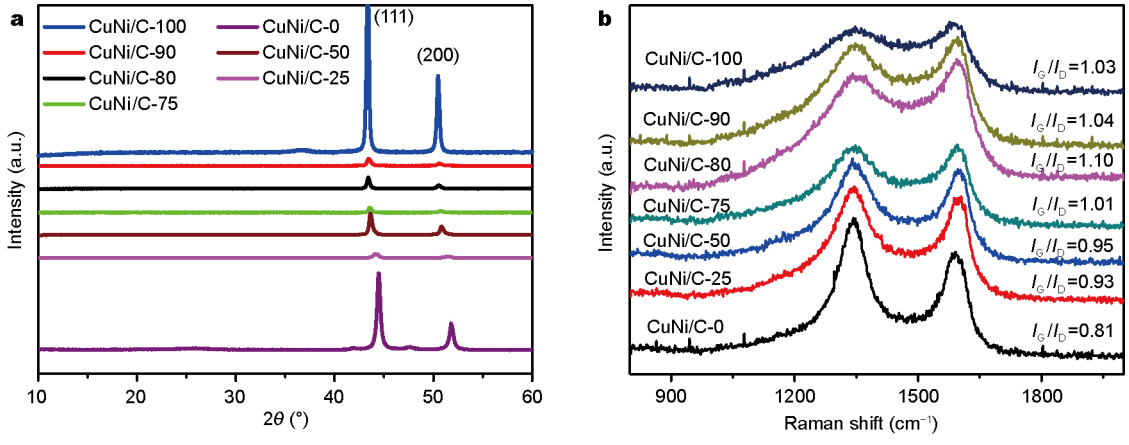

Figure 2 (a) XRD patterns of the MOF-derived CuNi/C-n. (b) Raman spectra for CuNi/C-n.

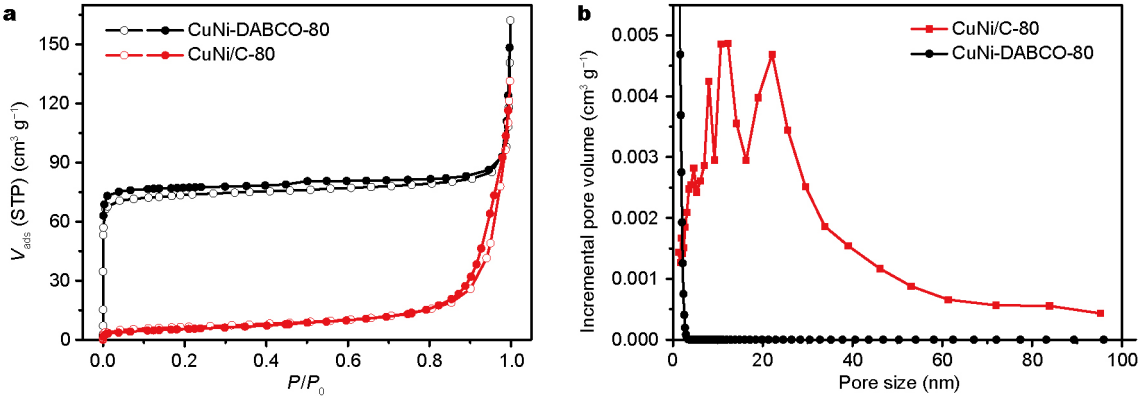

Figure 3 (a) N_2 sorption isotherms at 77 K of CuNi-DABCO-80 (black) and CuNi/C-80 (red). (b) Corresponding pore size distribution plots.

of CuNi/C-80 during the pyrolysis. The majority of pores remain in the micropore range, while the pore size increases to a certain degree and mesopores appear. This pore enlargement is due to the thermal rupture of micropores and gaseous evaporation at the fairly high temperature. The presence of different kinds of pores with various sizes provides good diffusion access for oxygen to reach the active sites, which raises the oxygen reduction catalytic efficiency.

In order to assess the oxygen reduction catalytic performance of the bimetallic carbon-based catalysts, RDE measurements were conducted in the O_2-saturated alkaline system at a scan rate of 10 mV s^{-1}, and K-L equations were used to evaluate the electron transfer efficiency. The CV curves for all samples (Fig. 4a and Fig. S4) exhibit a distinct oxygen reduction peak starting at ca. 0.7 V in the O_2-saturated electrolytes compared with the Ar-saturated system, demonstrating the ORR catalytic activity of the designed bimetallic carbon-based materials. Some of the curves for both Ar-and O_2-initial conditions also show peaks ca. 0.2 V (Fig. 4a and Fig. S4a, c, f). These peaks can be attributed to the reduction from CuO to Cu(0) [36,49], indicating partial oxidization of the samples during preservation. The LSV curves collected on the RDE of different CuNi/C-n samples at 1600 rpm are displayed in Fig. 4b to investigate the optimal metal ratio for ORR catalysis. Compared to each other, the monometallic samples exhibit clear advantages—a large current density for Cu/C and a higher onset potential for Ni/C. As expected, most of the CuNi/C-n samples present much better catalytic performance, as they take advantage of both metals. Remarkably, CuNi/C-80 presents the largest current density (5.34 mA cm^{-2}) and the most positive onset potential (0.73 V, same for CuNi/C-90), and both values are enhanced compared with Ni/C and Cu/C. Also, these two samples possess the highest half-wave potential of 0.61 V while the second-top value is 0.6 V for CuNi/C-0, 25 and 75. These results are all useful pieces of evidence for achieving the ultimate goal of this work, which is to verify the feasibility and effectiveness of combining the advantages of different metals with a facile synthesis method. Fig. 4c illustrates the K-L plots at different potentials. The electron transfer number, *n*, was calculated based on the linear K-L equation (Equations 1–3). Taking CuNi/C-80 as the representative, the values of *n* for CuNi/C-n and Cu/C are ca. 4.0, which is similar to that of commercial Pt/C, indicating a dominant four-electron ORR process. Comparatively, Ni/C favors a two-electron pathway despite its higher onset potential. Together with the positively-shifted onset potential, this result suggests that the bimetallic carbon nanocomposites inherit the advantages of both metal elements, resulting in even better electrocatalytic performance. Such ORR catalysis enhancement should be attributed to the synergetic effect of the two metal elements, uniform distribution, high surface area and graphitized carbon support.

In addition to the catalytic activity enhancement, the CuNi/C-n material also exhibits excellent stability in alkaline conditions. Two sets of LSV data were collected before and after 1000 continuous potential cycles, from 0.86 to 0.46 V at a scan rate of 10 mV s^{-1}, in O_2-saturated 0.1 mol L^{-1} KOH. As shown in Fig. 4e, the CuNi/C-80 presents only a slight current density loss and a slight negative shift in onset potential (7 mV). In contrast, Pt/C experiences a distinct negative shift of 44 mV (Fig. 4f). The results here demonstrate the strong stability of the designed CuNi/C-n material, making it a reliable catalyst approaching the performance of Pt/C.

CONCLUSIONS

In summary, we successfully synthesized bimetallic MOFs

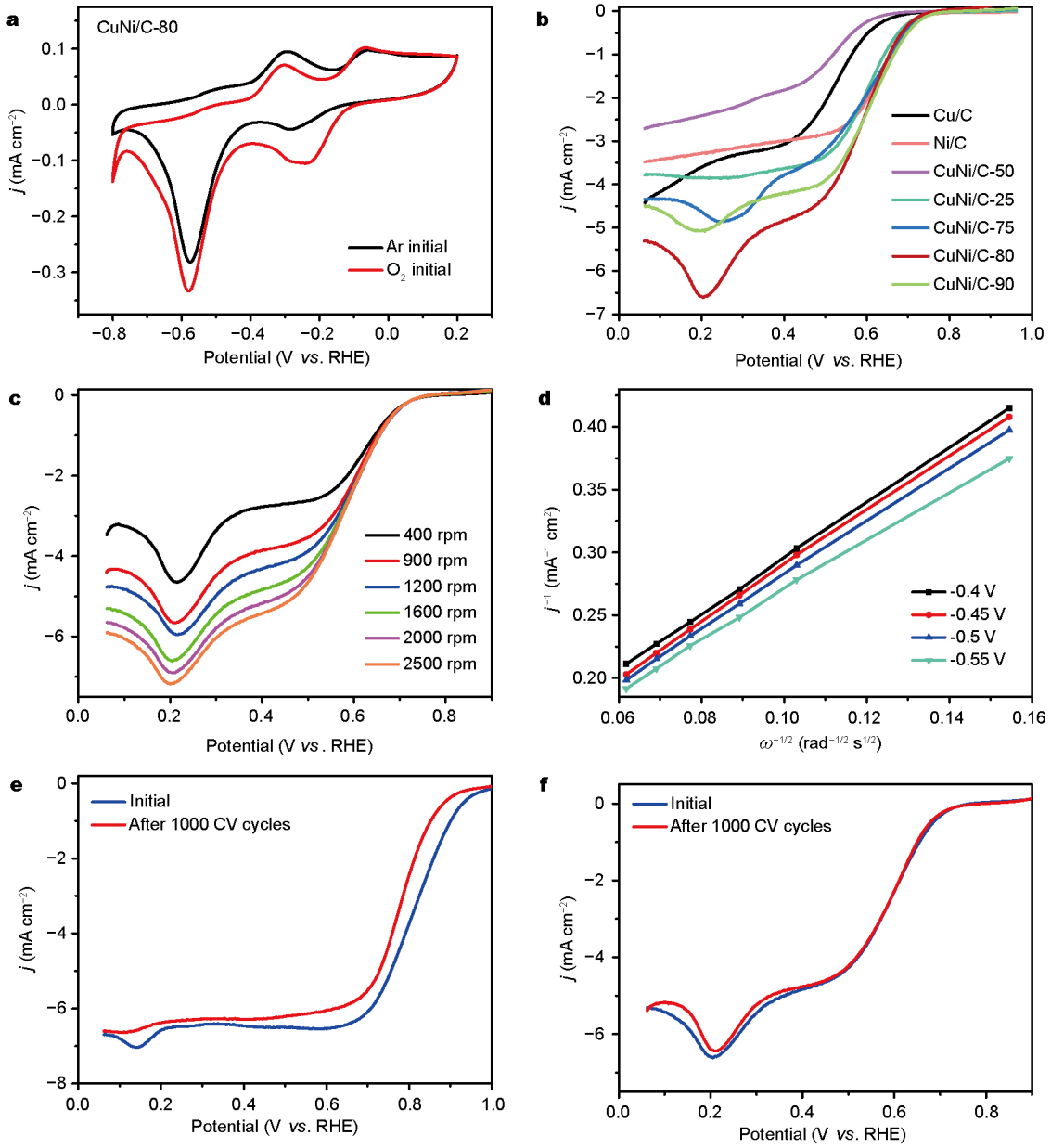

Figure 4 (a) CV curves of CuNi/C-80 in Ar- and O_2- saturated 0.1 mol L^{-1} KOH. (b) LSV curves for CuNi/C-n in O_2-saturated 0.1 mol L^{-1} KOH at the rotation rate of 1600 rpm. (c) LSV curves for CuNi/C-80 at different rotation speeds. (d) K-L plots of CuNi/C-80 at different potentials. LSV curves for (e) CuNi/C-80 and (f) commercial Pt/C before and after 1000 continuous potential cycles between −0.4 and 0 V in O_2-saturated 0.1 mol L^{-1} KOH.

CuNi-DABCO-n as precursors to bimetallic carbon nanocomposites (CuNi/C-n) with controllable metal ratios. The MOF-derived CuNi/C obtains a nanoscale particle size, high surface area and graphitic carbon from the precursor, which benefits subsequent ORR catalytic activity. Among the prepared series of samples, the CuNi/C-80 presented the best ORR catalytic activity with the largest current density, and the highest onset and half-wave potentials. It incorporates the advantages, and exceeds the performance, both of its monometallic constituents, Cu/C and Ni/C. Similar to that observed for Pt/C, the electron transfer number, n, of CuNi/C-80 (~ 4.0) is indicative of an efficient four-electron pathway. In addition, the high current density retention and slight negative shift in onset potential indicate that the CuNi/C-n materials have good stability in alkaline solution, making them reliable catalysts that approach the performance of Pt/C. The optimized ORR catalytic performance can be attributed to

the synergetic effect of the two metal elements, uniform elemental distribution, high surface area, and a graphitized carbon matrix. This method of combining the advantages of several elements to fabricate a material with improved performance has the potential to be extended to other systems. It also shows much promise for discovering alternatives to Pt-based catalysts for the use in energy storage and conversion systems.

Received 24 February 2017; accepted 2 May 2017; published online 16 May 2017

1 Ge X, Sumboja A, Wuu D, *et al.* Oxygen reduction in alkaline media: from mechanisms to recent advances of catalysts. ACS Catal, 2015, 5: 4643–4667
2 Shao M, Chang Q, Dodelet JP, *et al.* Recent advances in electrocatalysts for oxygen reduction reaction. Chem Rev, 2016, 116: 3594–3657
3 Liang Y, Li Y, Wang H, *et al.* Co_3O_4 nanocrystals on graphene as a synergistic catalyst for oxygen reduction reaction. Nat Mater, 2011, 10: 780–786
4 Chen S, Wang L, Wu Q, *et al.* Advanced non-precious electrocatalyst of the mixed valence CoO_x nanocrystals supported on N-doped carbon nanocages for oxygen reduction. Sci China Chem, 2015, 58: 180–186
5 Chen Z, Higgins D, Yu A, *et al.* A review on non-precious metal electrocatalysts for PEM fuel cells. Energ Environ Sci, 2011, 4: 3167
6 Hou Y, Wen Z, Cui S, *et al.* An advanced nitrogen-doped graphene/cobalt-embedded porous carbon polyhedron hybrid for efficient catalysis of oxygen reduction and water splitting. Adv Funct Mater, 2015, 25: 872–882
7 Shang C, Li M, Wang Z, *et al.* Electrospun nitrogen-doped carbon nanofibers encapsulating cobalt nanoparticles as efficient oxygen reduction reaction catalysts. ChemElectroChem, 2016, 3: 1437–1445
8 Wang B. Recent development of non-platinum catalysts for oxygen reduction reaction. J Power Sources, 2005, 152: 1–15
9 Liu Y, Liu Y, Cheng SHS, *et al.* Conformal coating of heterogeneous CoO/Co nanocomposites on carbon nanotubes as efficient bifunctional electrocatalyst for Li-air batteries. Electrochim Acta, 2016, 219: 560–567
10 Wang W, Shi Y, Li M, *et al.* Ultrafine N-doped carbon nanoparticles with controllable size to enhance electrocatalytic activity for oxygen reduction reaction. RSC Adv, 2016, 6: 110758–110764
11 Yi QF, Zhang YH, Liu XP, *et al.* Carbon-supported Fe/Co-N electrocatalysts synthesized through heat treatment of Fe/Co-doped polypyrrole-polyaniline composites for oxygen reduction reaction. Sci China Chem, 2014, 57: 739–747
12 Li S, Ding L, Fan L. Electrochemical synthesis of sulfur-doped graphene sheets for highly efficient oxygen reduction. Sci China Chem, 2015, 58: 417–424
13 Xia BY, Yan Y, Li N, *et al.* A metal–organic framework-derived bifunctional oxygen electrocatalyst. Nat Energ, 2016, 1: 15006
14 Chen YZ, Wang C, Wu ZY, *et al.* From bimetallic metal-organic framework to porous carbon: high surface area and multicomponent active dopants for excellent electrocatalysis. Adv Mater, 2015, 27: 5010–5016
15 Li L, Dai P, Gu X, *et al.* High oxygen reduction activity on a metal–organic framework derived carbon combined with high degree of graphitization and pyridinic-N dopants. J Mater Chem A, 2017, 5: 789–795
16 Xia W, Mahmood A, Liang Z, *et al.* Earth-abundant nanomaterials for oxygen reduction. Angew Chem Int Ed, 2016, 55: 2650–2676
17 Guan BY, Yu L, (David) Lou XW. A dual-metal–organic-framework derived electrocatalyst for oxygen reduction. Energ Environ Sci, 2016, 9: 3092–3096
18 Cao YL, Lv FC, Yu SC, *et al.* Simple template fabrication of porous $MnCo_2O_4$ hollow nanocages as high-performance cathode catalysts for rechargeable Li-O_2 batteries. Nanotechnology, 2016, 27: 135703
19 Liu Y, Wang M, Cao LJ, *et al.* Interfacial redox reaction-directed synthesis of silver@cerium oxide core–shell nanocomposites as catalysts for rechargeable lithium–air batteries. J Power Sources, 2015, 286: 136–144
20 Ma Z, Kyotani T, Liu Z, *et al.* Very high surface area microporous carbon with a three-dimensional nano-array structure: synthesis and its molecular structure. Chem Mater, 2001, 13: 4413–4415
21 Ryoo R, Joo SH, Kruk M, *et al.* Ordered mesoporous carbons. Adv Mater, 2001, 13: 677–681
22 Lee J, Kim J, Hyeon T. Recent progress in the synthesis of porous carbon materials. Adv Mater, 2006, 18: 2073–2094
23 Jiao Y, Zheng Y, Jaroniec M, *et al.* Origin of the electrocatalytic oxygen reduction activity of graphene-based catalysts: a roadmap to achieve the best performance. J Am Chem Soc, 2014, 136: 4394–4403
24 Stock N, Biswas S. Synthesis of metal-organic frameworks (MOFs): routes to various MOF topologies, morphologies, and composites. Chem Rev, 2012, 112: 933–969
25 Zhang E, Xie Y, Ci S, *et al.* Multifunctional high-activity and robust electrocatalyst derived from metal–organic frameworks. J Mater Chem A, 2016, 4: 17288–17298
26 Férey G. Hybrid porous solids: past, present, future. Chem Soc Rev, 2008, 37: 191–214
27 Liu C, Wang J, Li J, *et al.* Electrospun ZIF-based hierarchical carbon fiber as an efficient electrocatalyst for the oxygen reduction reaction. J Mater Chem A, 2017, 5: 1211–1220
28 Zheng R, Liao S, Hou S, *et al.* A hollow spherical doped carbon catalyst derived from zeolitic imidazolate framework nanocrystals impregnated/covered with iron phthalocyanines. J Mater Chem A, 2016, 4: 7859–7868
29 Seredych M, Rodriguez-Castellon E, Bandosz TJ. New Cu_xS_y /nanoporous carbon composites as efficient oxygen reduction catalysts in alkaline medium. J Mater Chem A, 2014, 2: 20164–20176
30 Hu H, Han L, Yu M, *et al.* Metal–organic-framework-engaged formation of Co nanoparticle-embedded carbon@Co_9S_8 double-shelled nanocages for efficient oxygen reduction. Energ Environ Sci, 2016, 9: 107–111
31 Fu T, Fang J, Wang C, *et al.* Hollow porous nanoparticles with Pt skin on a Ag–Pt alloy structure as a highly active electrocatalyst for the oxygen reduction reaction. J Mater Chem A, 2016, 4: 8803–8811
32 Zeng X, You C, Leng L, *et al.* Ruthenium nanoparticles mounted on multielement co-doped graphene: an ultra-high-efficiency cathode catalyst for Li–O_2 batteries. J Mater Chem A, 2015, 3: 11224–11231
33 Baioni AP, Vidotti M, Fiorito PA, *et al.* Synthesis and characterization of copper hexacyanoferrate nanoparticles for building up long-term stability electrochromic electrodes. Langmuir, 2007, 23: 6796–6800
34 Brüller S, Liang HW, Kramm UI, *et al.* Bimetallic porous porphyrin polymer-derived non-precious metal electrocatalysts for oxygen reduction reactions. J Mater Chem A, 2015, 3: 23799–23808

35 Liu Y, Liu Y, Shi H, *et al.* Cobalt-copper layered double hydroxide nanosheets as high performance bifunctional catalysts for rechargeable lithium-air batteries. J Alloys Compd, 2016, 688: 380–387
36 Ania CO, Seredych M, Rodriguez-Castellon E, *et al.* New copper/GO based material as an efficient oxygen reduction catalyst in an alkaline medium: the role of unique Cu/rGO architecture. Appl Catal B-Environ, 2015, 163: 424–435
37 Bhagi-Damodaran A, Michael MA, Zhu Q, *et al.* Why copper is preferred over iron for oxygen activation and reduction in haem-copper oxidases. Nat Chem, 2016, 9: 257–263
38 Solomon EI, Sundaram UM, Machonkin TE. Multicopper oxidases and oxygenases. Chem Rev, 1996, 96: 2563–2606
39 Cracknell JA, Vincent KA, Armstrong FA. Enzymes as working or inspirational electrocatalysts for fuel cells and electrolysis. Chem Rev, 2008, 108: 2439–2461
40 Rosado G, Verde Y, Valenzuela-Muñiz AM, *et al.* Catalytic activity of Pt-Ni nanoparticles supported on multi-walled carbon nanotubes for the oxygen reduction reaction. Int J Hydrogen Energ, 2016, 41: 23260–23271
41 Arán-Ais RM, Dionigi F, Merzdorf T, *et al.* Elemental anisotropic growth and atomic-scale structure of shape-controlled octahedral Pt–Ni–Co alloy nanocatalysts. Nano Lett, 2015, 15: 7473–7480
42 Bu L, Ding J, Guo S, *et al.* A general method for multimetallic platinum alloy nanowires as highly active and stable oxygen reduction catalysts. Adv Mater, 2015, 27: 7204–7212
43 Chaemchuen S, Zhou K, Kabir NA, *et al.* Tuning metal sites of DABCO MOF for gas purification at ambient conditions. Microporous Mesoporous Mater, 2015, 201: 277–285
44 Chen H, Wang D, Yu Y, *et al.* A surfactant-free strategy for synthesizing and processing intermetallic platinum-based nanoparticle catalysts. J Am Chem Soc, 2012, 134: 18453–18459
45 Sun J, Liu H, Chen X, *et al.* Carbon nanorings and their enhanced lithium storage properties. Adv Mater, 2013, 25: 1125–1130
46 Guo L, Jiang WJ, Zhang Y, *et al.* Embedding Pt nanocrystals in N-doped porous carbon/carbon nanotubes toward highly stable electrocatalysts for the oxygen reduction reaction. ACS Catal, 2015, 5: 2903–2909
47 Maldonado-Hódar FJ, Moreno-Castilla C, Rivera-Utrilla J, *et al.* Catalytic graphitization of carbon aerogels by transition metals. Langmuir, 2000, 16: 4367–4373
48 Khan IA, Qian Y, Badshah A, *et al.* Highly porous carbon derived from MOF-5 as a support of ORR electrocatalysts for fuel cells. ACS Appl Mater Interfaces, 2016, 8: 17268–17275
49 Jayalakshmi M, Balasubramanian K. Cyclic voltammetric behavior of copper powder immobilized on paraffin impregnated graphite electrode in dilute alkali solution. Int J Electrochem Sci, 2008, 3: 1277–1287

Acknowledgments This work was supported by the National Natural Science Foundation of China (21671096 and 21603094), the Natural Science Foundation of Shenzhen (JCYJ20150630145302231 and JCYJ20150331101823677), and the Science and Technology Innovation Foundation for the Undergraduates of SUSTech (2014S07, 2016S10 and 2016S20).

Author contributions Wu S, Cao L, Cheng H and Lu Z designed and conceived the research framework; Wu S, Zhu Y, Huo Y, Luo Y prepared and engineered the samples; Wu S, Zhu Y, Huo Y, Luo Y, Zhang L, Wan Y and Nan B conducted the performance investigation; Wang Z, Li M and Yang M conducted the characterizations; Wu S wrote the paper with support from Lu Z.

Conflict of interest The authors declare that they have no conflict of interest.

Supplementary information Supporting data are available in the online version of this paper.

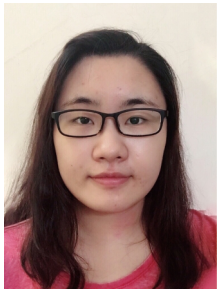

Sisi Wu received her BE degree in material science & engineering from Southern University of Science and Technology in 2016. She started a joint PhD at both National University of Singapore and Southern University of Science and Technology in 2017, under the supervision of Prof. Qing Wang and Prof. Zhouguang Lu. Her research interests are focused on the development of cathode materials and redox molecules for Li-air batteries.

Zhouguang Lu is currently an associate professor in the Department of Materials Science and Engineering, Southern University of Science and Technology, China. He received his PhD degree from City University of Hong Kong in 2009. He is the recipient of Fulbright Fellowship of USA Government in 2008–2009 and the Overseas High-Caliber Personnel (Level B) of Shenzhen Government in 2013. His research mainly covers the design and synthesis of nanostructures and their applications in energy storage and conversion with focus on lithium/sodium -ion and -air batteries. He has authored more than 100 peer-review journal papers with total citations more than 2800 and H-index of 30.

双金属有机骨架衍生CuNi/C纳米复合型高效氧还原催化剂的研究

吴思思, 朱迎港, 霍一峰, 罗耀聪, 张丽华, 万弋, 南博, 曹鲁杰, 王振宇, 李泯婵, 杨明阳, 程化, 卢周广*

摘要 氧还原催化剂在金属空气电池和燃料电池的可再生能源技术中起至关重要的作用. 尽管该方面研究已有很多, 高活性低成本的催化剂的开发仍然十分困难. 本文以金属有机骨架为前驱体, 成功合成出非贵金属铜镍双金属碳基纳米复合物并作为高效的氧还原催化剂. 单金属复合物Cu/C和Ni/C皆具有较好的氧还原催化作用, 铜镍双金属复合物进一步综合了二者优点从而提升了催化性能. 本文所合成的铜镍双金属复合物中的金属比例可通过调整前驱体中的原料配比来准确控制, 所得的一系列金属比例的铜镍双金属碳基纳米复合物在极限电流密度、起始电位和半波电位三个方面都超过了单金属复合物. 此外, 铜镍双金属碳基纳米复合物在碱性环境中具有良好的稳定性且超过了目前最好的氧还原催化材料铂, 大大加强了其作为氧还原催化剂的优势. 铜镍双金属碳基纳米复合物优越的电化学催化性能归功于金属铜和镍以及碳材料基底的协同作用.